ORIGINAL PAPER

Use of the airborne magnetic data for edge basalt detection in Qaret Had El Bahr area, Northeastern Bahariya Oasis, Egypt

Mahmoud Elhussein[1] · Mohamed Shokry[2]

Abstract

In this study, different interpretation techniques have been applied to the airborne magnetic data to detect the subsurface basaltic edges in Qaret Had El Bahr area, Northeastern Bahariya Oasis, Egypt. These techniques are as follows: the power spectrum, Source Parameter Imaging (SPI), tilt derivative or tilt angle, Euler deconvolution, and forward modeling. The depth to the basement calculated from the different techniques is mostly matched. Also, the lineaments have been analyzed by extracting these lineaments from the geological map, Reduction to the Pole (RTP) magnetic map, and regional and residual magnetic map. The rose diagrams of these lineaments have been established to define the main trends in the study area as well as the trend of the basalt, which is the main target in this study.

Keywords RTP · SPI · Tilt angle · Depth estimation

Introduction

Our area of interest (study area) (Fig. 1) lies in the Western Desert, to the Northeastern Bahariya Oasis, Egypt. It is bounded by latitudes 28°00′ and 29°15′ N and longitudes 29°00′ and 30°00′ E. The aeromagnetic survey is very useful in delineating or mapping subsurface magnetic sources (Elkhodary and Youssef 2013). Aeromagnetic measurements are routinely presented in form of maps constituting magnetic anomaly of interest that are produced from sources with different geometric, located at various depths (Salawu et al. 2019a; Salawu et al. 2019b).

Aeromagnetic maps can be applied in many earth science studies such as geothermal, hydrological archeological, hydrocarbon, and mineral investigations (Reford and Sumner 1964; Mehanee and Zhdanov 2002; Zhdanov et al. 2004; Paoletti et al. 2013; Mehanee 2014; Pei et al. 2014; Eppelbaum 2015; Essa and Elhussein

2016; Maineult 2016). Central to the analyses and interpretation of aeromagnetic maps is the estimation of magnetic basement depths (Deng et al. 2016; Salawu et al. 2019b), outlining the lateral changes in the magnetic susceptibilities (Oruç and Selim 2011), delineating the structural features (Al-Garni 2010; Gabtni et al. 2016), and recording the Curie depths (Aboud et al. 2011).

This research is mainly committed to find and outline subsurface sources (basaltic sheet) and their extensions, considering the fact that the study area is along the TransAfrican basalt lineament and also situated between two of six exposed Egyptian Oligocene volcanic basalts. Analytical signal (total gradient), tilt angle, Source Parameter Imaging (SPI), and the 3D Euler deconvolution are standard tools used to map structural features and to estimate the depths of magnetized bodies within the study area (Al-Garni 2010). Additionally, two geomagnetic models were constructed to display the subsurface basement reliefs and their structural control.

✉ Mahmoud Elhussein
mahmoudelnouishy@yahoo.com

[1] Geophysics Department, Faculty of Science, Cairo University, P.O. 12613, Giza, Egypt

[2] Nuclear Materials Authority, P.O. Box 530, Maadi, Cairo, Egypt

Geologic setting

The study area which lies in the Western Desert, to the Northeastern Bahariya Oasis, Egypt, is covered with a variety of sedimentary rocks ranging in age from Late Cretaceous to Quaternary (Fig. 2a). Upper cretaceous
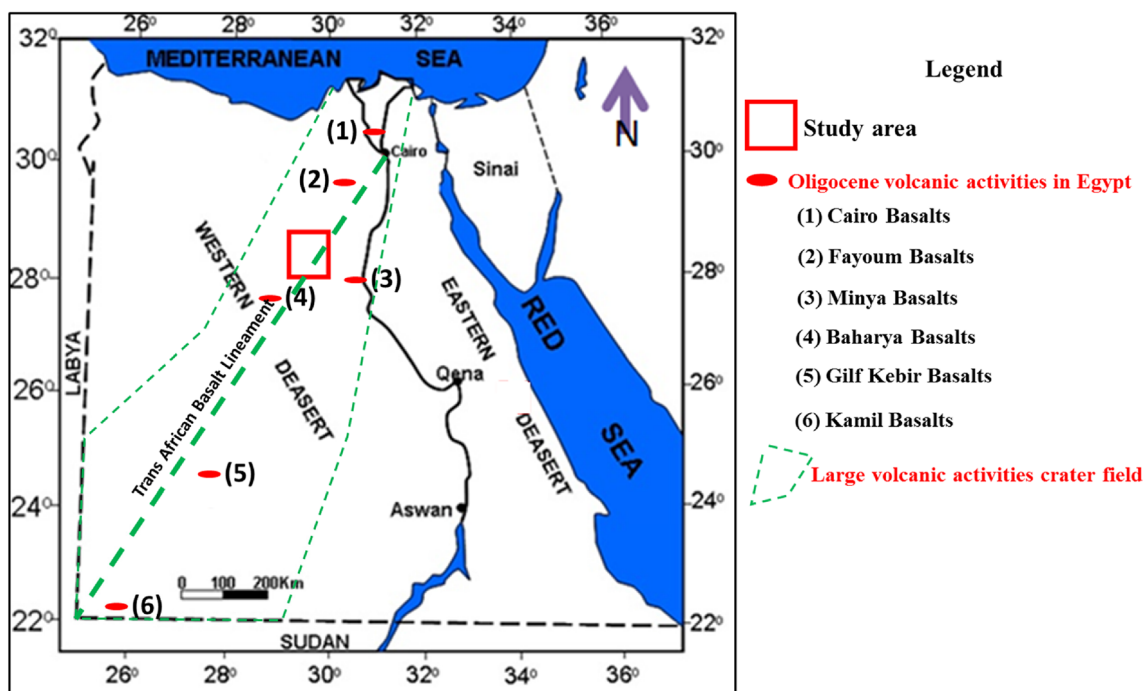
Fig. 1 Location map of Qaret Had El Bahr area, Northeastern Bahariya Oasis, Egypt, and sketch layout of Oligocene volcanic activities in Egypt

rocks cover the southwestern part of the area and represent the Bahariya Formation (Kub) and El Heiz Formation (Kuz). Bahariya Formation (Kub) consists of intercalations of ferruginous sandstone and siltstone. Meanwhile, El Heiz Formation (Kuz) is shallow marine limestone and dolomite in the upper and lower members, enclosing between them a clastic carbonate section. The northern Tertiary sequence in the Faiyum area is shown in Fig. 2b. The Eocene sedimentary rocks cover more than 50% of the exposed surface geology. The Upper Eocene section consists of Qasr El Sagha Formation (Tes), Abu Maharek Formation (Tea), and Homra Formation (Temh). Qasr El Sagha appears northeast and southwest of the study area; Abu Maharek Formation (Tea) is composed of claystone and silty marl with limestone intercalation; it is shown at the south central part of the study area (Fig. 2a). Homra Formation (Temh) is composed of silty limestone with shale intercalation and appears at the central part of the study area and extends from the northeastern to the southwestern parts. Middle Eocene consists of Rayan Formation (Temr) and Qazzun Formation (Temq). Rayan Formation is composed of marl intercalated with burrowed sandstone and appears at the northeastern part of the study area. Qazzun Formation (Temq) is composed of white platform limestone and is shown at the west central part of the study area. Meanwhile, the Lower Eocene is located at the southwestern part of the study area and is represented by Minia Formation (Tel) and Naqb Formation (Teln). Minia Formation (Tel) is composed of well-bedded lagoonal

limestone; Naqb Formation (Teln) is composed of fossiliferous limestone with minor shale intercalations.

The Oligocene Gabal Qatrani Formation (Toq) is situated at the western part of the study area and structures a sequence of continental to marine altering clastics (brownish siltstone and ruddy claystone), as well as topped with the Egyptian Tertiary basalts (Widan el-Faras Formation) which lies above the Qatrani Formation. It was first portrayed by Beadnell (1905) in the El-Faiyum depression. These Tertiary basalt sheets which uncovered at Widan el-Faras and Gabal Qatrani are subdivided from top to base as pursues: Cavities rich altered basalt layer filled by auxiliary calcite and halite pockets; vesicular basalt appearing dull green somewhat blue shading, and vesicles filled by calcite and sulfur; olivine basalt, having a pale to dim green shading, hard to extremely hard with sulfur filling cracks. Qatrani Formation is underlain by unconformably basalt flows (Kusky et al. 2011).

The Miocene sedimentary rock is represented by the Moghra Formation (Tmg) at the northern part of the study area. It is composed of continental to shallow marine clastic sequence, including shale and white sandy carbonate. As well as Quaternary wadi deposits (sand dunes (Qd) and gravels (Qg)) are spread as narrow widths and long lengths trending NNW-SSE (Conoco 1986), structurally, the lineaments have been extracted from the geological map, including the NE-SW, NW-SE, N-S, and E-W directions. These trends almost define a number of tectonic parts of different dip regimes.
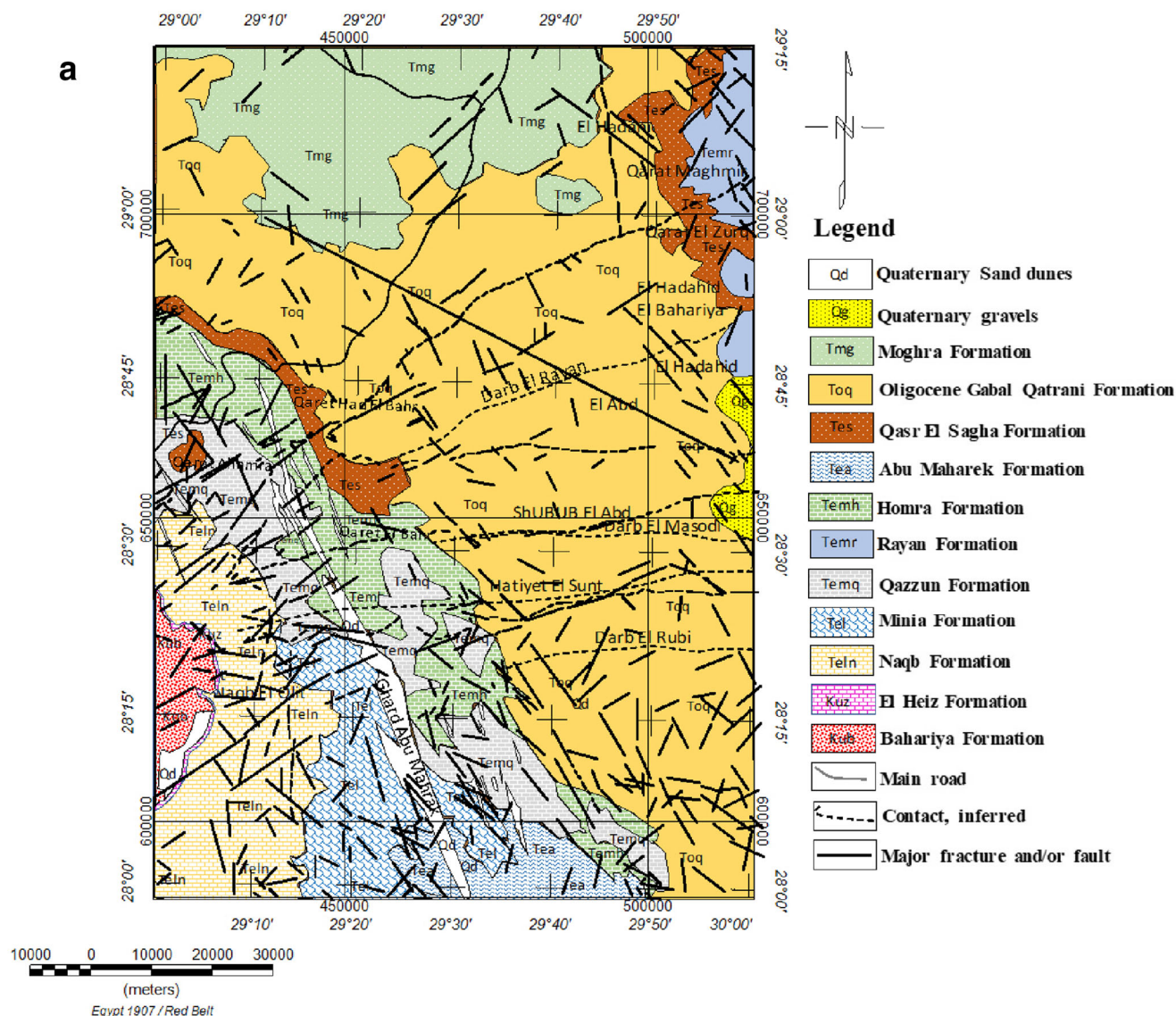
Fig. 2 **a** Geological map of Qaret Had El Bahr area, Northeastern Bahariya Oasis, Egypt. **b** Tertiary sequence in the Faiyum area (from Beadnell (1905), as modified by said (1962) and Vondra (1974))

Data sources and processing

The aeromagnetic anomaly data of the study area are available through the MPGAP project (cooperation between the Egyptian General Petroleum Corporation (EGPC), the Egyptian Geological Survey and Mining Authority (EGSMA), and Aero-Service Division, Western Geophysical Company of America). In 1982, this cooperation performed an airborne magnetic over a huge part of the Eastern Desert with some parts of the central Western Desert of Egypt, in order to provide data which assist in identifying and evaluating minerals, petroleum, and groundwater resources of the region (Aero-Service 1984). The traverse lines took N45° E direction, with spacing of 1.5 km approximately. The tie lines were perpendicular to the traverse lines (took N135° E

direction) and spaced with about 10 km. The station separation was 92.65 m; the average ground speed of the aircraft ranged from 222 to 314 km/h with a mean terrain clearance of 120 m.

The total magnetic intensity data (TMI) were gridded using Geosoft Oasis Montaj software; the *x*-point separation and *y*-point separation are 423.2 m (Fig. 3).

We applied different standard transformation techniques to the aeromagnetic anomaly data in order to map structural features, to estimate depths to sources, and to provide 2D subsurface pictorial view of the region under study. These techniques are discussed in the next section ("Methodology"). The software used to process and enhance the data was the Geosoft Oasis Montaj (Oasis Montaj 2009).

b

AGE			SEQUENCE	THICKNESS
MIOCENE			Kashab Formation	>100 m
			- - - - erosional unconformity - - - -	
OLIGOCENE	Late		Widan el Faras Basalt[1]	0–10 m
			- - - erosional unconformity - - - - (2 or more?)	
	Early		Widan el Faras Basalt[2]	0–15 m
			- - - - erosional unconformity - - - -	
			Jebel Qatrani Formation	340 m
			conformable to minor erosional unconformity	
EOCENE	Late	Qasr el Sagha Formation	Dir Abu Lifa Member (new)	77 m
			- - - erosional unconformity - - -	
			Temple Member (new)	123 m
			Birket Qarun Formation	50 m
	Middle		Gehannam Formation (ravine beds)	70 m
			Wadi Rayan Formation	130 m

Fig. 2 (continued)

Methodology

Reduction to magnetic pole

Reduction to the north magnetic pole (RTP) filter has been applied to the total magnetic intensity data of the study area (the used inclination (I) was 41.2° and the used declination (D) was 2°), in order to expel the inclination and declination impacts of the earth's magnetic field. The RTP makes magnetic interpretation easy since it repositions the magnetic anomalies over their sources (Li 2008), provided that the direction of the magnetization vector is known. The resulting RTP aeromagnetic anomaly map is shown in Fig. 4.

Regional-residual separation using matched filtering

Power spectrum analysis is one of the useful tools for determining the average depths of magnetic sources, which can help in finding the magnetic horizons within the crust (Spector and Grant 1970; Reddi et al. 1988; Rama Rao et al. 2011; Selim and Aboud 2012). It is a plot of the source amplitude logarithm versus wavenumber (Spector and Grant 1970). Firstly, the data must be applied to the Fast Fourier transform, before calculating the average power spectrum.

A typical power spectrum composed of three sources: a deep-seated regional component, which has a low frequency; a shallow residual component, which has a higher frequency; and the noise component (Fig. 5a); each of these components can be shown as a straight line (Ogunmola et al. 2016) that represent different subsurface geologic layers (Salawu et al. 2019b). These components can be separated by bandpass filters according to wavelength (Sheriff 2010). Figure 5b shows the depth estimate of the different components in Fig. 5a. The depths of the regional and residual components can be calculated using the following formula:

$$h = -s/4\pi \quad (1)$$

where h is the depth and s is the slope of the straight line, which represents the source.

By applying the power spectrum (Fig. 5a), the regional (Fig. 6) and residual (Fig. 7) components were
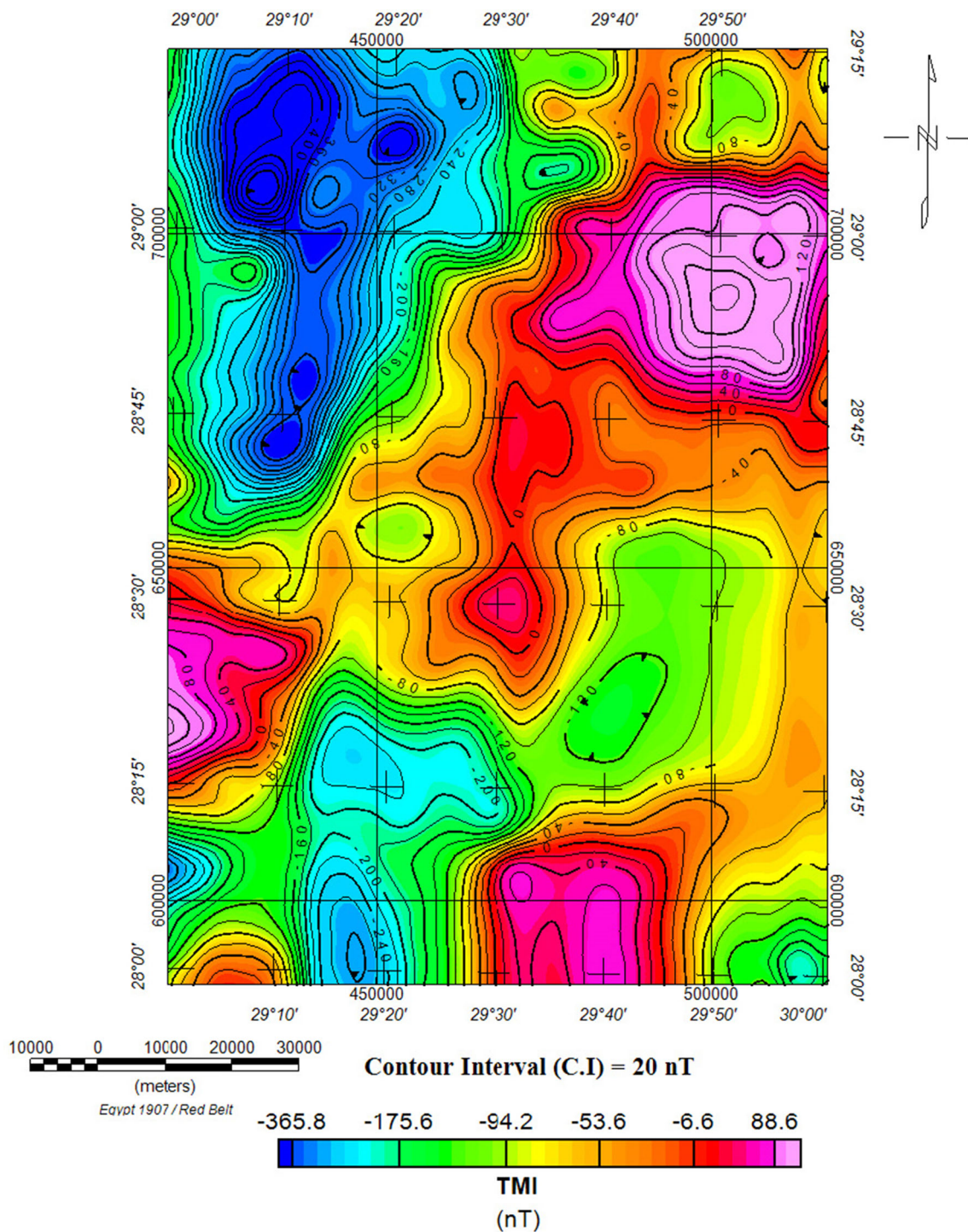
Fig. 3 Total magnetic intensity (TMI) map of Qaret Had El Bahr area, Northeastern Bahariya Oasis, Egypt

separated, using a bandpass filter, at which the low wavenumber cutoff and the high wavenumber cutoff for the regional component are 0.0021 and 0.04, respectively, while the low wavenumber cutoff and the high wavenumber cutoff for the residual component are 0.04 and 0.15, respectively. Depth calculated from this technique using Eq. 1 for the regional component is 4720 m, and the depth of the residual component is 1830 m.

Source Parameter Imaging

Thurston and Smith (1997) developed a technique called Source Parameter Imaging (SPI); this technique is based upon
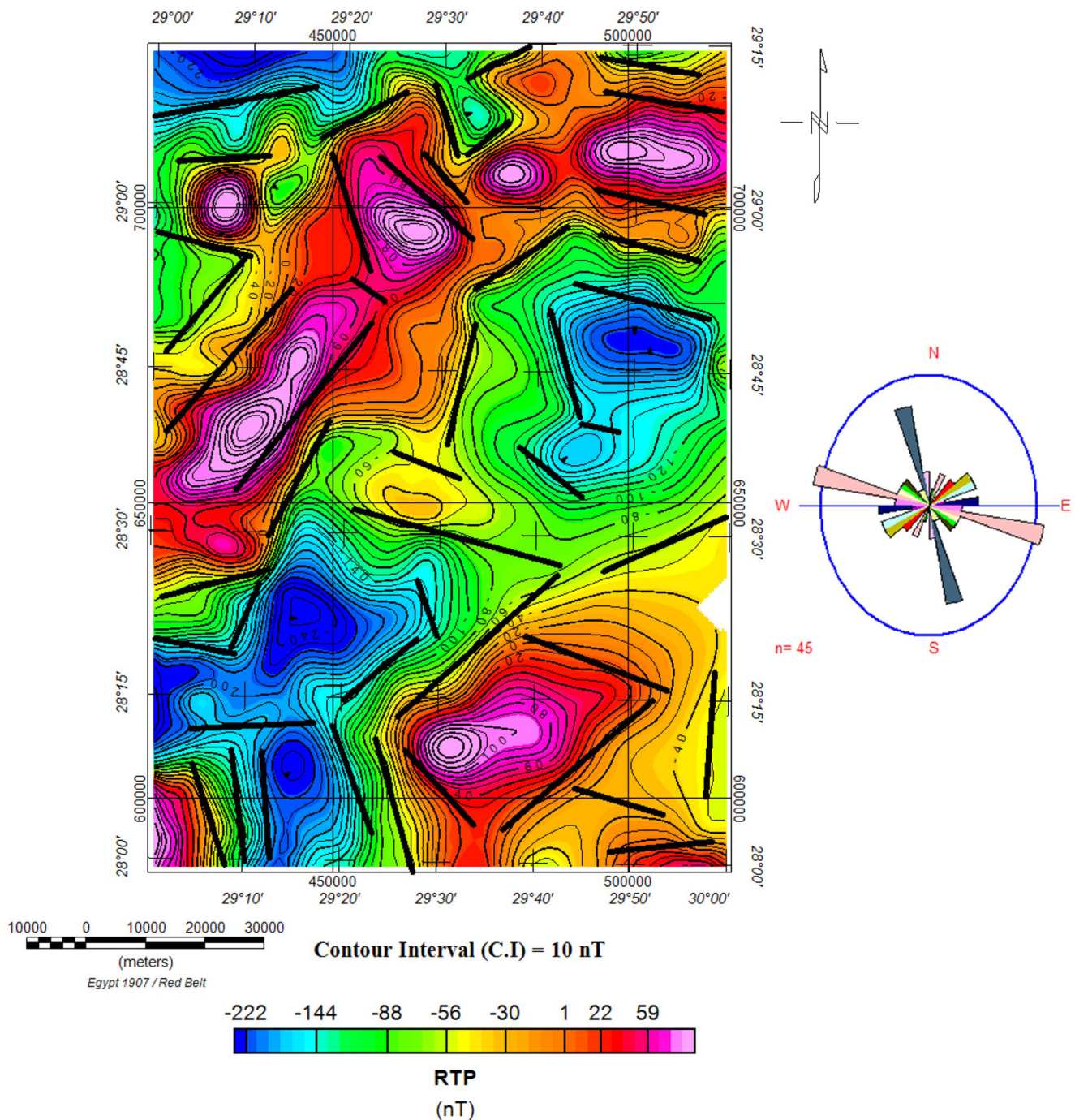
Fig. 4 RTP magnetic map of Qaret Had El Bahr area, Northeastern Bahariya Oasis, Egypt, with the extracted lineaments and the rose diagram showing main trends

the extension of complex analytical signal, in order to determine the depths of magnetic sources. In this method, the depth of magnetic source is related to the local wavenumber (k) of the magnetic field (Ogunmola et al. 2016; Fairhead et al. 2004), which can be computed from the horizontal and vertical gradients of the RTP (Reduction to the Pole) grid. The local wavenumber function is given by the following formula (Al-Badani and Al-Wathaf 2017):

$$k(x,y) = \frac{\dfrac{\partial^2 T}{\partial x \partial z}\dfrac{\partial T}{\partial x} + \dfrac{\partial^2 T}{\partial y \partial z}\dfrac{\partial T}{\partial y} + \dfrac{\partial^2 T}{\partial^2 z}\dfrac{\partial T}{\partial z}}{\left(\dfrac{\partial T}{\partial x}\right)^2 + \left(\dfrac{\partial T}{\partial y}\right)^2 + \left(\dfrac{\partial T}{\partial z}\right)^2}, \qquad (2)$$

where k is local wavenumber and $\frac{\partial T}{\partial x}, \frac{\partial T}{\partial y}, \frac{\partial T}{\partial z}$ are the first horizontal derivative of field T in x direction, the first
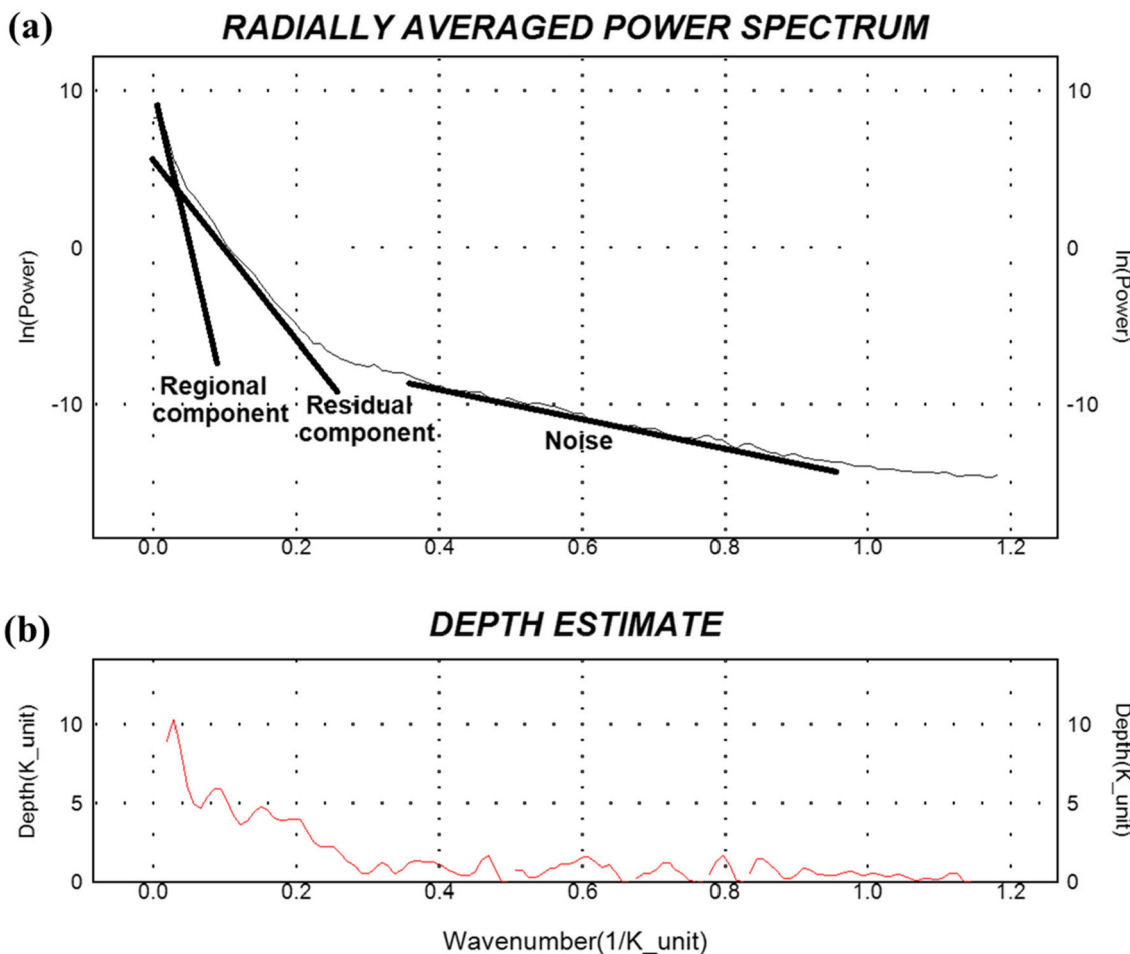
Fig. 5 **a** Power spectrum separation technique showing regional, residual, and noise component. **b** Depth estimated from Fig. 5a using the power spectrum technique

horizontal derivative of field T in y direction, and the first vertical derivative of Field T in z direction, respectively. The depth of magnetic source can be calculated from the following formula (Al-Badani and Al-Wathaf 2017):

$$z_{x=0} = \frac{1}{k_{max}}, \qquad (3)$$

where $z_{x=0}$ is the estimated depth at the source edge and k_{max} is the peak value of the local wavenumber over the step source.

Tilt angle

The tilt angle technique, proposed by Miller and Singh (1994), is calculated through the SPI method, using Geosoft Oasis Montaj. This method is based upon the total horizontal derivative and vertical derivative of the field, to calculate the depth of magnetic sources. The following formula represents the tilt angle applied to grid data (Verduzco et al. 2004):

$$TDR = \theta = tan^{-1}\left(\frac{\frac{\partial T}{\partial z}}{\sqrt{\left(\frac{\partial T}{\partial x}\right)^2 + \left(\frac{\partial T}{\partial y}\right)^2}}\right), \qquad (4)$$

where $\frac{\partial T}{\partial x}, \frac{\partial T}{\partial y}, \frac{\partial T}{\partial z}$ are the first horizontal derivative of the field T in x direction, the first horizontal derivative of the field T in y direction, and the first vertical derivative of the field T in z direction.

The values of tilt angle ranges from $-\pi/2$ to $\pi/2$ rad. The tilt angle reaches 0 at or close to the edge of a vertical-sided source and is negative away from the source (Miller and Singh 1994). The depth to the edge of the magnetized source can be calculated, using the tilt angle technique, by measuring the distance between 0 and $\pm \pi/4$ contours (or half the distance between the $+ \pi/4$ and $- \pi/4$ contours) (Salem et al. 2007).
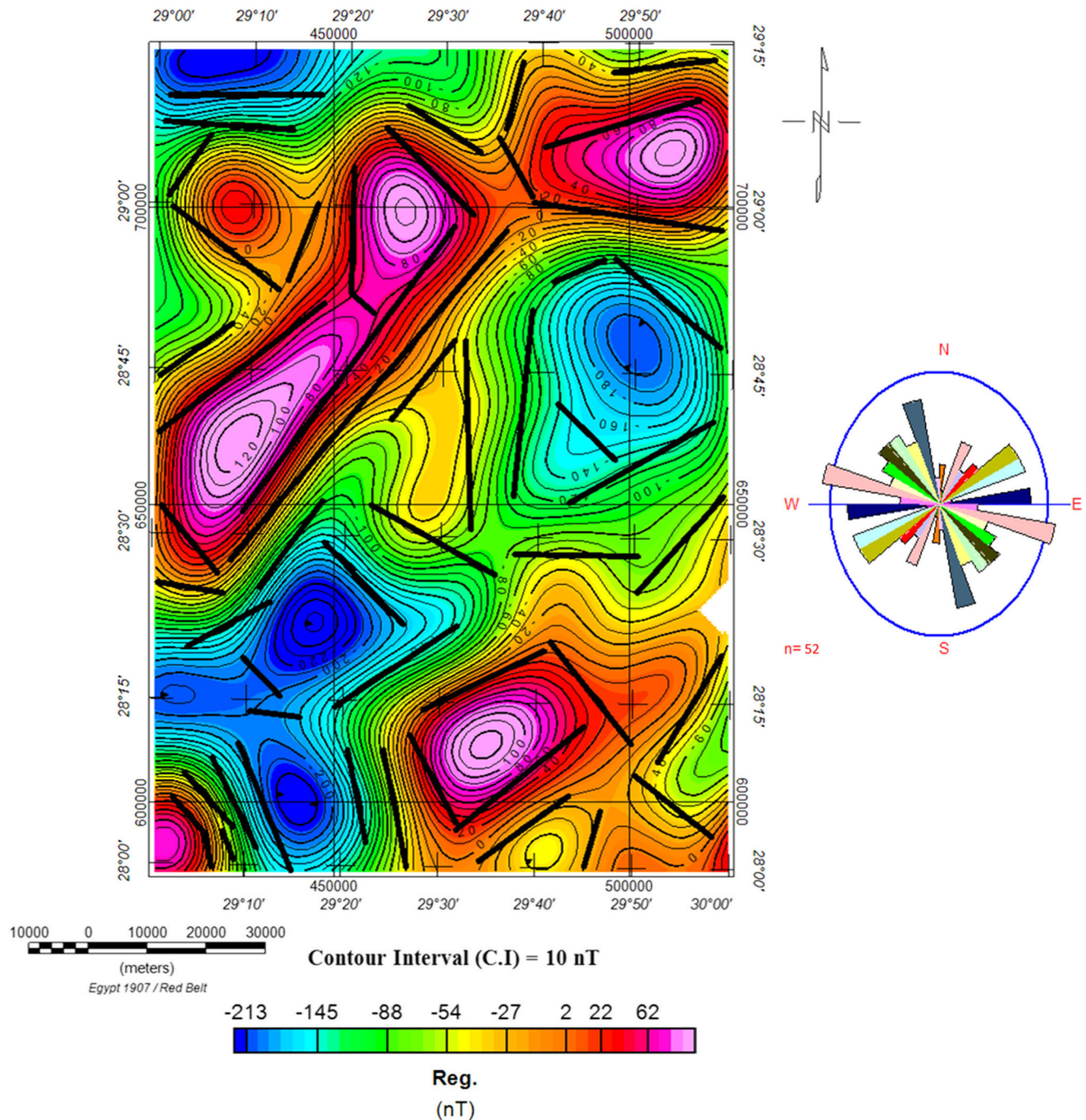
Fig. 6 Regional magnetic map of the study area separated from RTP magnetic data by using power spectrum technique, and the extracted lineaments with the rose diagram showing main trends

Total gradient (TG) technique

Total gradient method is a successful technique to detect the edges of magnetic sources (Roset et al. 1992; Roest and Pilkington 1993; Salawu et al. 2019b). The total gradient can be calculated from the following formula (Roset et al. 1992; Salawu et al. 2019b):

$$TG = \sqrt{\left(\frac{\partial T}{\partial x}\right)^2 + \left(\frac{\partial T}{\partial y}\right)^2 + \left(\frac{\partial T}{\partial z}\right)^2}, \quad (5)$$

where TG is the total gradient, T is the magnetic field, and $\frac{\partial T}{\partial x}$, $\frac{\partial T}{\partial y}$, $\frac{\partial T}{\partial z}$: are the first horizontal derivative of field T in x
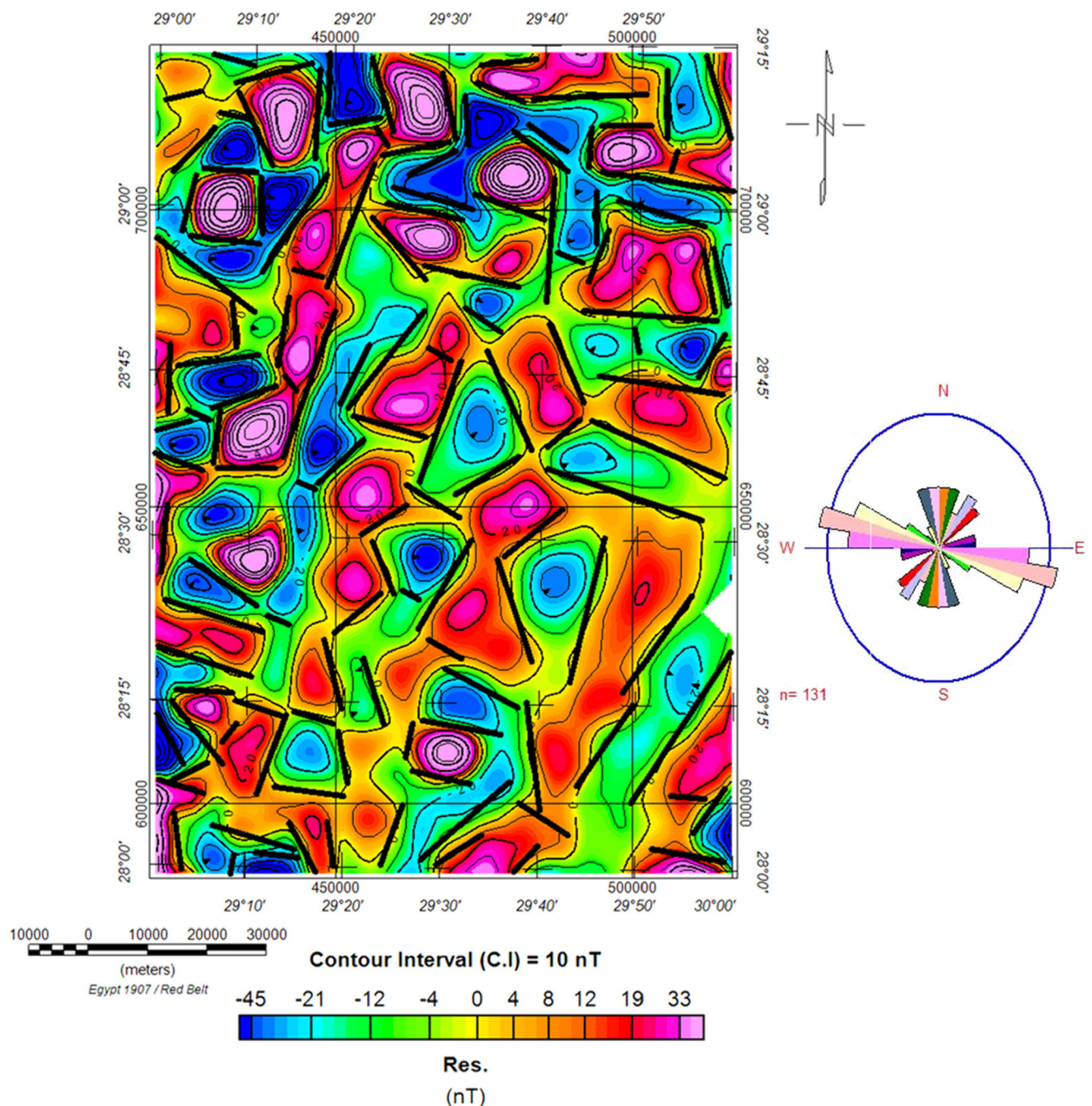
Fig. 7 Residual magnetic map of the study area separated from RTP magnetic map by using power spectrum technique, and the extracted Lineaments with the rose diagram showing main trends

direction, the first horizontal derivative of field T in y direction, and the first vertical derivative of Field T in z direction, respectively.

The maximum values of amplitude of the total gradient are located directly over the edges of the source bodies (Roset et al. 1992; Macleod et al. 1993; Selim 2016).

3D Euler deconvolution technique

The Euler deconvolution method was proposed by Thompson (1982), which is used to estimate the location of the different magnetic sources. The 3D Euler formula is given in the following formula (Thompson 1982; Reid et al. 1990):

$$(x-x_0)\frac{\partial T}{\partial x} + (y-y_0)\frac{\partial T}{\partial y} + (z-z_0)\frac{\partial T}{\partial z} = N\ (B-T), \qquad (6)$$

where x, y, and z are the observation point coordinates; x_0, y_0, and z_0 are the source location coordinates; and N is the attenuation rate or structural index (SI) which depends on the geometry of the source.

2.5D forward modeling

In order to determine the depth to the basement surface in the study area and the causes of sharp variation in the magnetic intensity, two magnetic models were constructed. In this study, the magnetic modeling involves four information, (1) top surface (basement depth), (2) bottom surface, (3) magnetic susceptibility (hidden objects), and (4) an anomaly (shift in magnetic amplitude). If three of
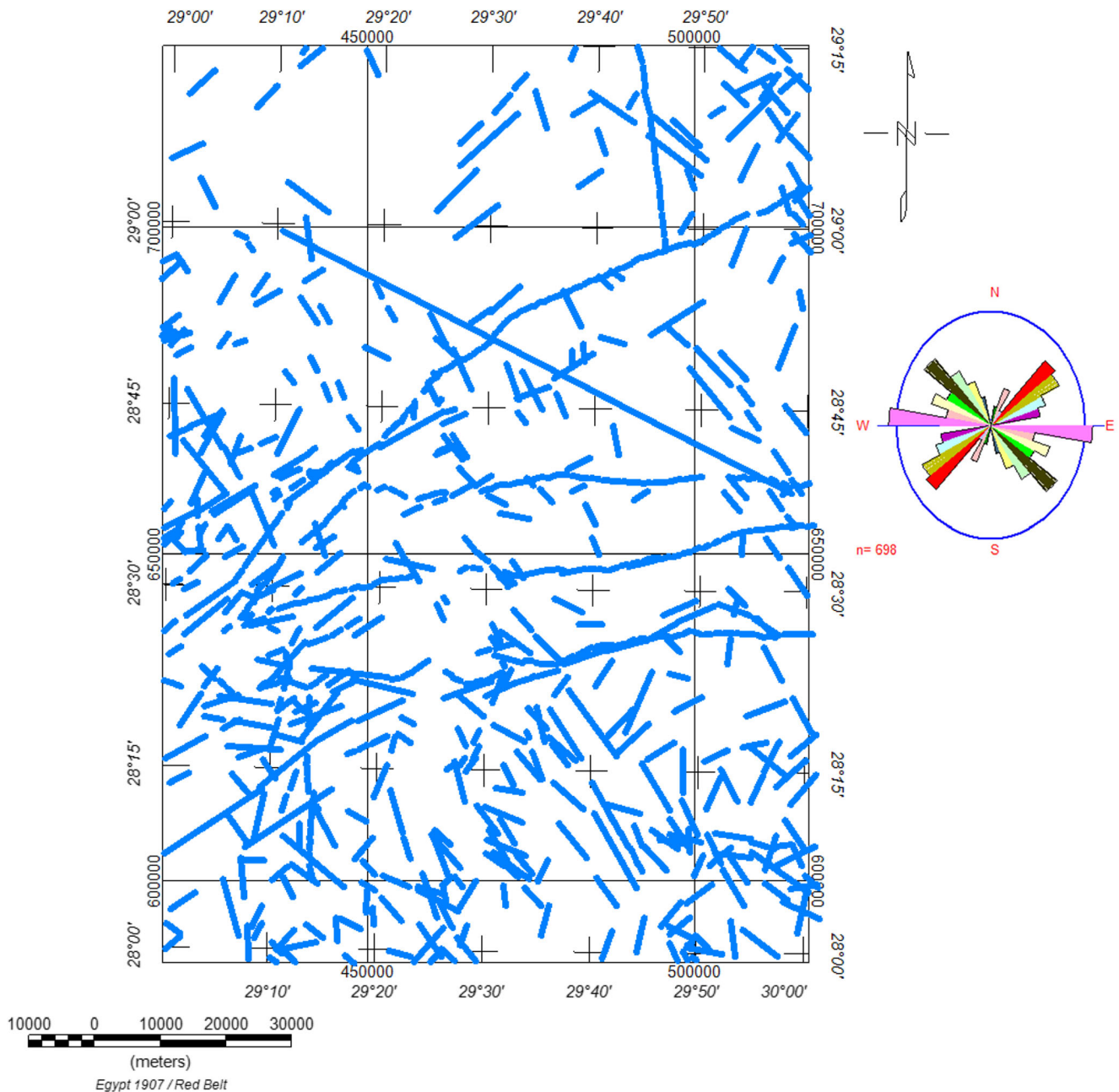

Fig. 8 Lineaments extracted from the geological map and rose diagram showing the main trends

this information are known or assumed, the fourth parameter may be compensated (El Sirafie 1986). Two magnetic anomaly profiles were taken from the RTP map in NW-SE direction (A1-A1' and A2-A2'); then the GM-SYS, Geosoft Oasis Montaj, was used to construct the two magnetic models. The models made by GM-SYS are based upon Talwani and Heirtzler (1964) algorithm, which relies on matching the magnetic effects of the n-sided polygonal body with that of the 2D arbitrary shaped body; the accuracy increases with increasing the number of polygonal sides (Selim 2016).

Results and discussion

First, the RTP magnetic map (Fig. 4) demonstrates a number of magnetic zones of varying intensities and different trends. The RTP map shows a wide range of magnetic values (from − 260 to 190 nT) and rapid changes in the density of contouring. The variation in the magnitude, direction, extent, and frequencies of the magnetic anomalies in the RTP map reflect different sources, depths, compositions, as well as tectonic settings (Saad et al. 2010). These high and low magnetic amplitudes are mostly caused by the integrated effect of both lithological (intra-basement) variations within the basement rocks and structural (supra-basement) variations out of the basement surface (Saad et al. 2010).

Then, the low negative anomalies of the RTP map that trend N-S, NE–SW, and WNW-ESE at the southwestern part of the study area may be related to low magnetic susceptibility of the intrusive materials, such as the acidic materials or large sedimentary section. Meanwhile, the two high positive anomalies of the RTP map that trend NE-SW and E-W at the northwestern, northeastern, and southeastern parts of the study area may be attributed to high magnetic susceptibility materials of the intrusive bodies, such as basic and ultrabasic dikes or uplifted basalts (Saad et al. 2010).

Fig. 9 Tilt angle map of Qaret Had El Bahr area, Northeastern Bahariya Oasis, Egypt, showing the location of basalt edges by white line
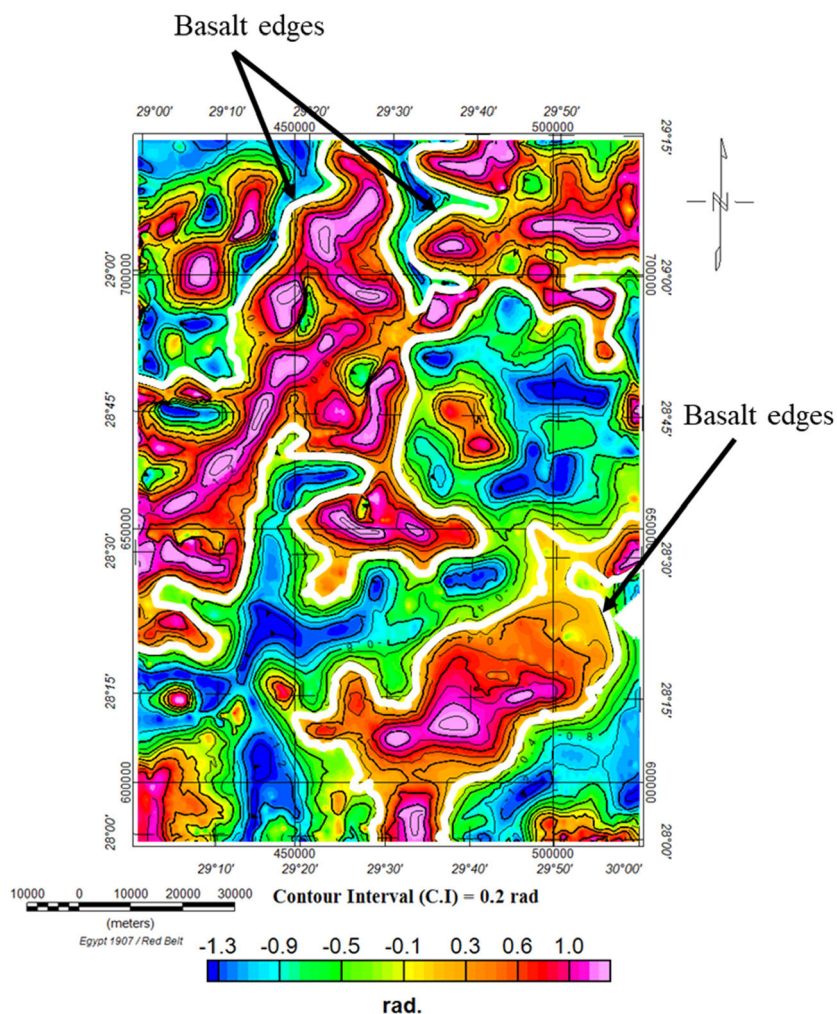
The follow-up basic dikes are observed clearly in deep roots through the regional map (Fig. 6), while the signatures of these dikes disappear and disintegrate to small fragments, gradually upward through the residual map (Fig. 7).

The lineaments have been extracted from the RTP, regional and residual magnetic, and geological maps (Figs. 4, 6, 7, and 8 respectively), in order to define the main trends in the study area. These maps can exhibit that there are four main trends: E-W, NW-SE, NE-SW, and N-S.

The second target is the edge detection of the basaltic igneous rock in the subsurface; this was achieved by applying the tilt angle and total gradient techniques to the RTP magnetic data. Figures 9 and 10 show the tilt angle and total gradient maps, respectively, which were used to define the edges and the position of the basalt sources. The basalt edges and positions are shown in Figs. 9 and 10, respectively, by white line.

Thirdly, the depth estimations of the basaltic igneous rocks were done by two different techniques; first, by applying the SPI method to RTP magnetic data, from the calculated SPI values, the depths of the magnetic sources in the study area range from 1857 m to 4000 m with mean depth about 2900 m (Fig. 11). Figure 11 shows the location of two boreholes: DIYUR-1 borehole, where the basement depth is 1625 m from drilling, and BAHARYIA-1 borehole, where the basement depth is about 1842 m. From the careful examination, it can be shown that, the depths of basaltic igneous intrusions in the subsurface range of more than 2000 m. The basalt extended in the NE-SW direction in the northwestern
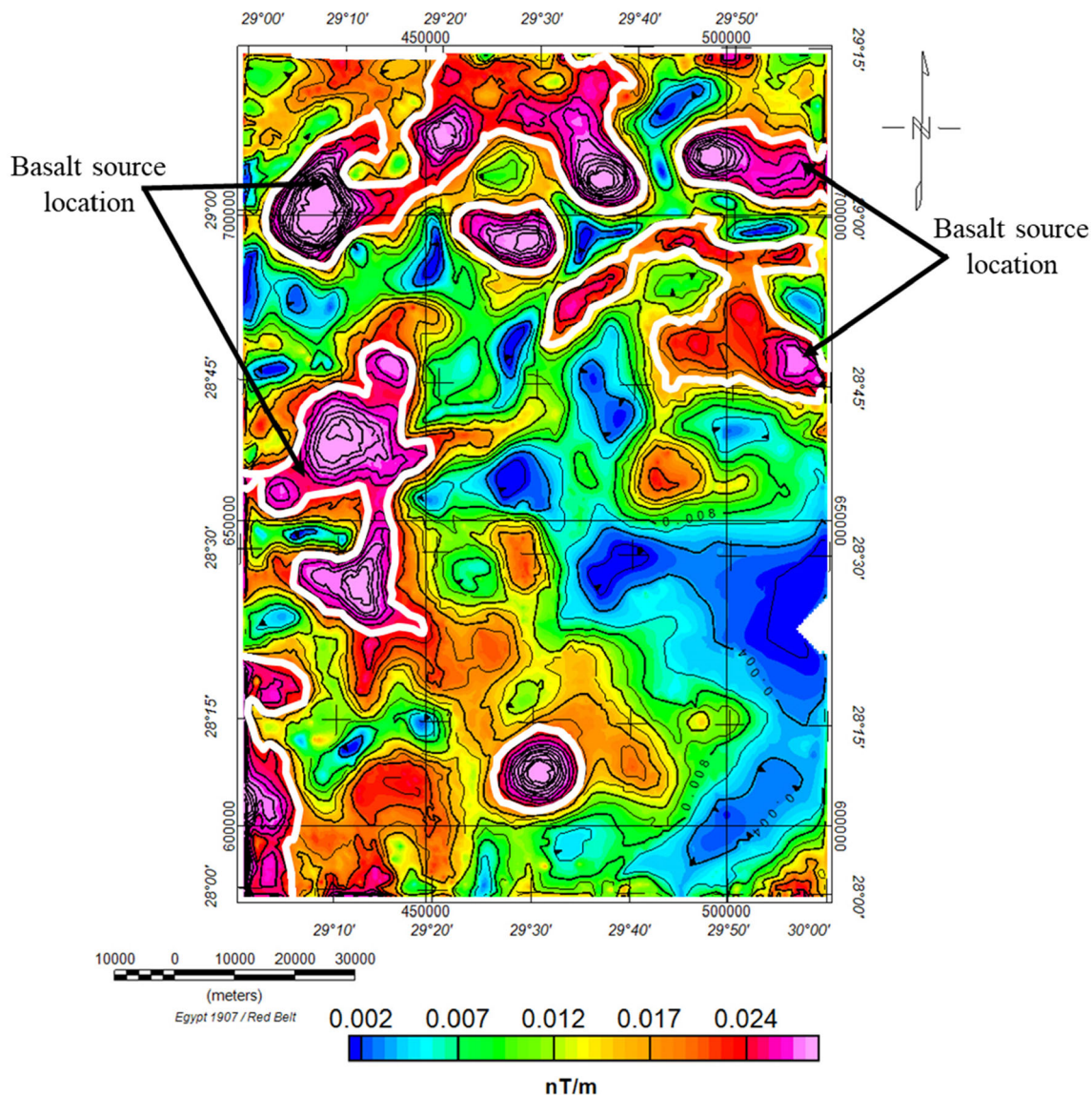

Fig. 10 Total gradient map of Qaret Had El Bahr area, Northeastern Bahariya Oasis, Egypt, showing the position of basalt sources by white line
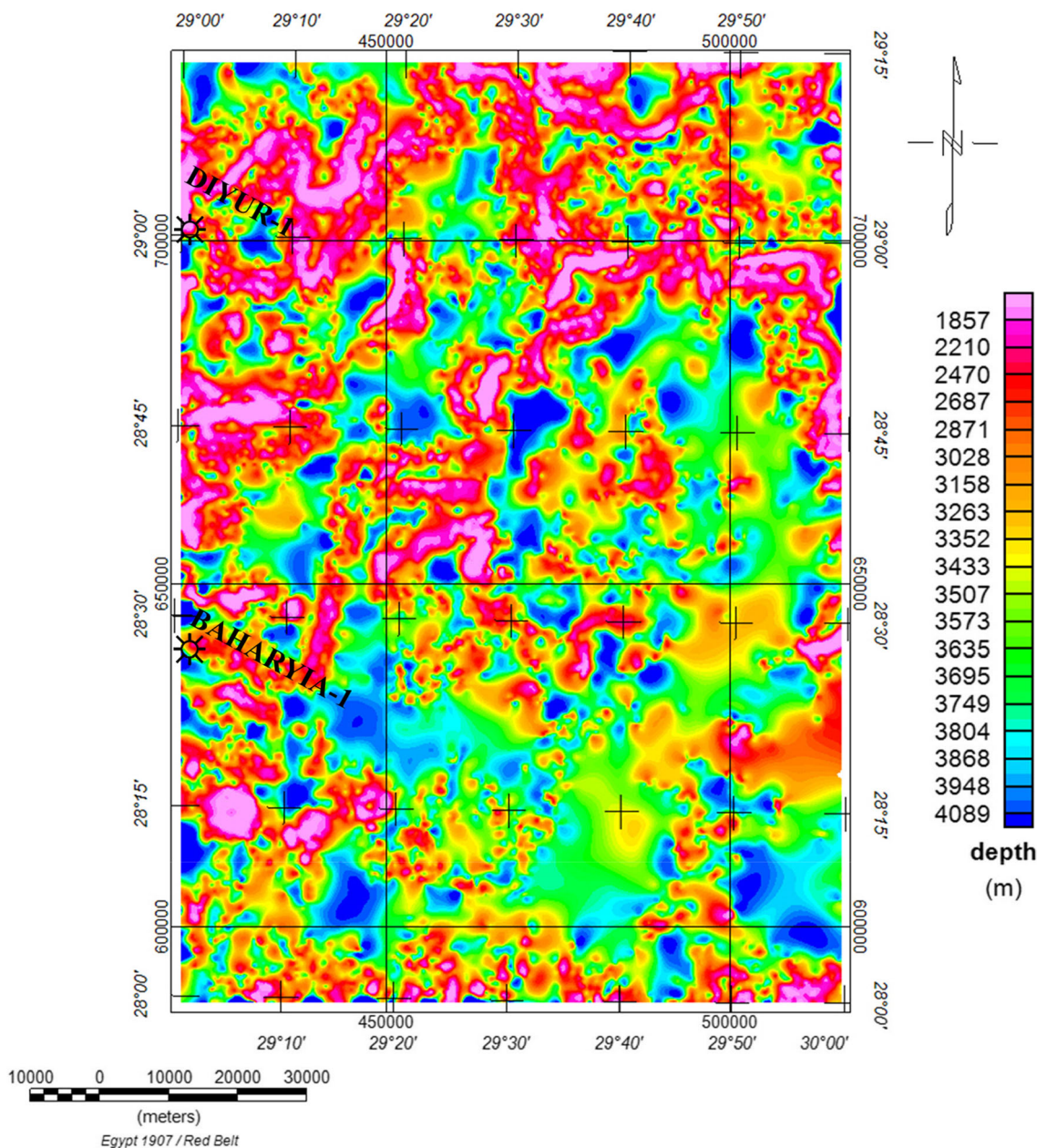
Fig. 11 Depth map of Qaret Had El Bahr area, Northeastern Bahariya Oasis, Egypt, calculated by the SPI (Source Parameter Imaging) technique, and the locations of the two boreholes (DIYUR-1 and BAHARYIA-1)

part of the map area. Secondly, by using the Euler deconvolution which has been applied to the RTP magnetic data, using SI = 1 for a dike model (Fig. 12), the depths calculated using the Euler deconvolution range from 1000 to 5000 m with mean depth of about 3150 m.

Finally, the diligence to determine the different depth ranges in the whole study area, two geomagnetic models were done for two profiles; as the forward modeling, the locations of these two profiles (A1-A1' and A2-A2') are shown in the RTP map (Fig. 13). The depths to the basement surface and the basement relief of the models are ranging from 1200 to 5080 m in the first model (Fig. 14)

and from 2210 to 5220 m in the second model (Fig. 15). Figures 14 and 15 show that, there are variation in the magnetic susceptibility of the basement which may be caused by fracturing, weathering, or faulting. The different geological lineaments which can explain these variations have been extracted from the regional map (Fig. 6).

Conclusions

In this study, we demonstrated the extension of basalt in the Bahariya area, using different interpretation methods
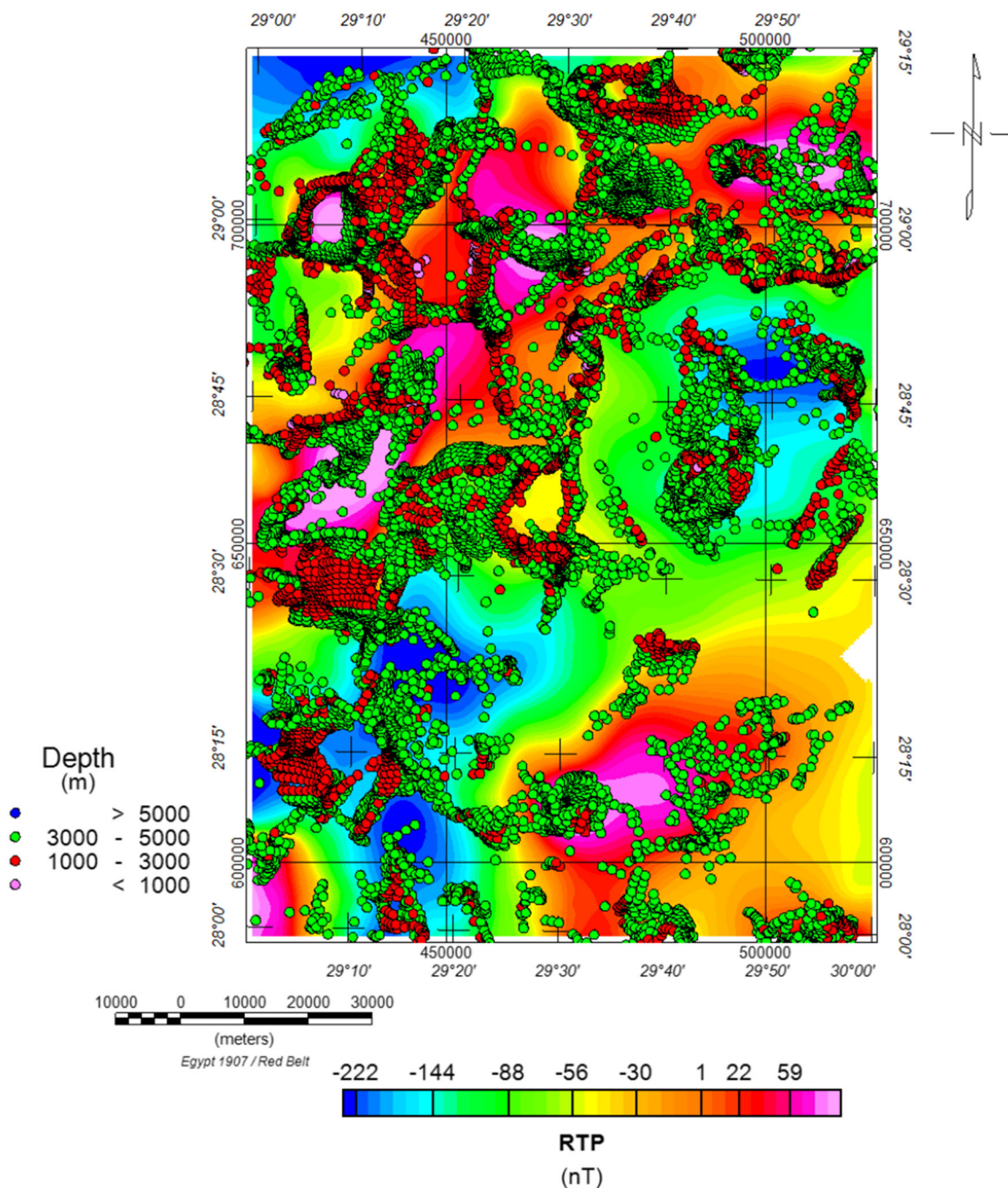
Fig. 12 Euler deconvolution depths posted on the RTP magnetic map

applied to the aeromagnetic data. The two high positive anomalies of the RTP map that trend NE-SW and E-W at the northwestern, northeastern, and southeastern parts of the study area may be attributed to high magnetic susceptibility materials of intrusive bodies, such as basic and ultrabasic dikes or uplifted basalt. The follow-up of basic dikes are observed clearly in deep roots at the regional map, while signatures of these dikes disappear and disintegrate into small bodies gradually upward at the residual map.

There are four main linear trends, i.e., E-W, NW-SE, NE-SW, and N-S, deduced from the geologic, RTP, regional, and residual maps. The magnetic anomalies related to basalt, which were detected from the tilt angle map, have a high magnetic intensity reach of about 190 nT. These anomalies are taking the NE-SW and E-W trends. Tilt angle and total gradient maps help to edge the horizontal and vertical contacts of the basic magma in the subsurface; these two maps show the basalt edges and positions by white lines. The depth of the regional

Fig. 13 Locations of the two magnetic profiles taken for geomagnetic modeling

Contour Interval (C.I) = 10 nT

-222　-144　-88　-56　-30　1　22　59

RTP

(nT)
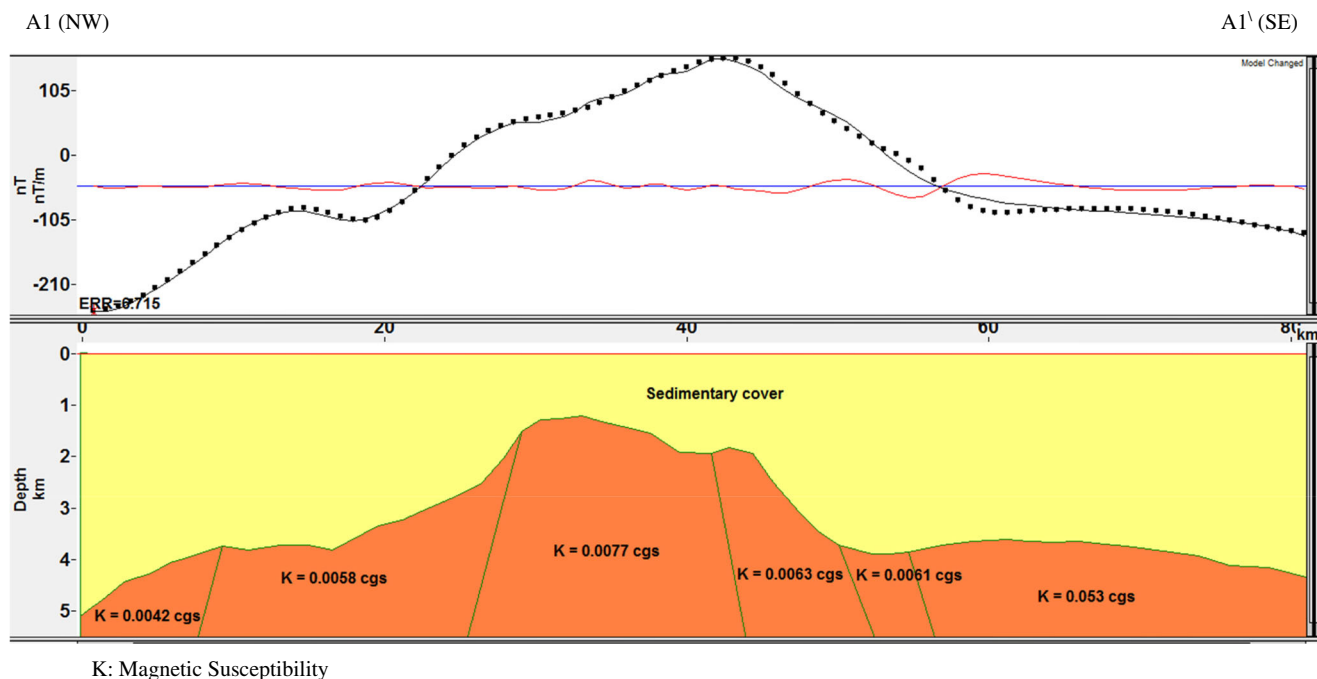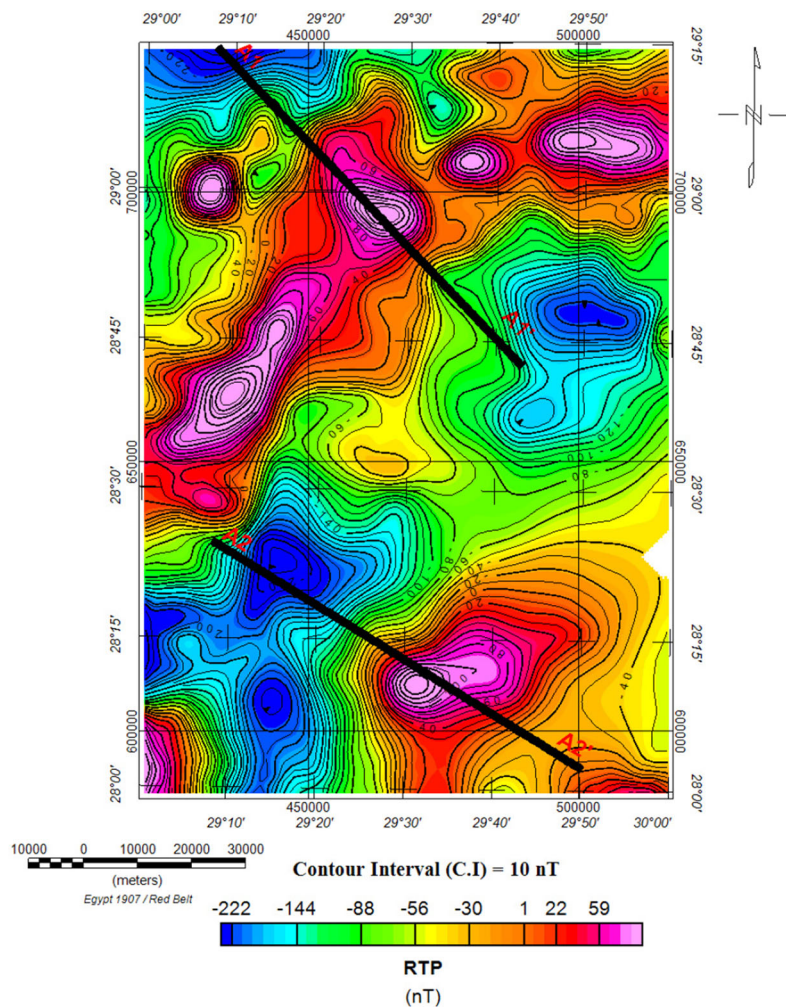
K: Magnetic Susceptibility

Fig. 14 2.5D model of the first profile A1-A1$^\backslash$

A2 (NW)   A2$^\backslash$ (SE)
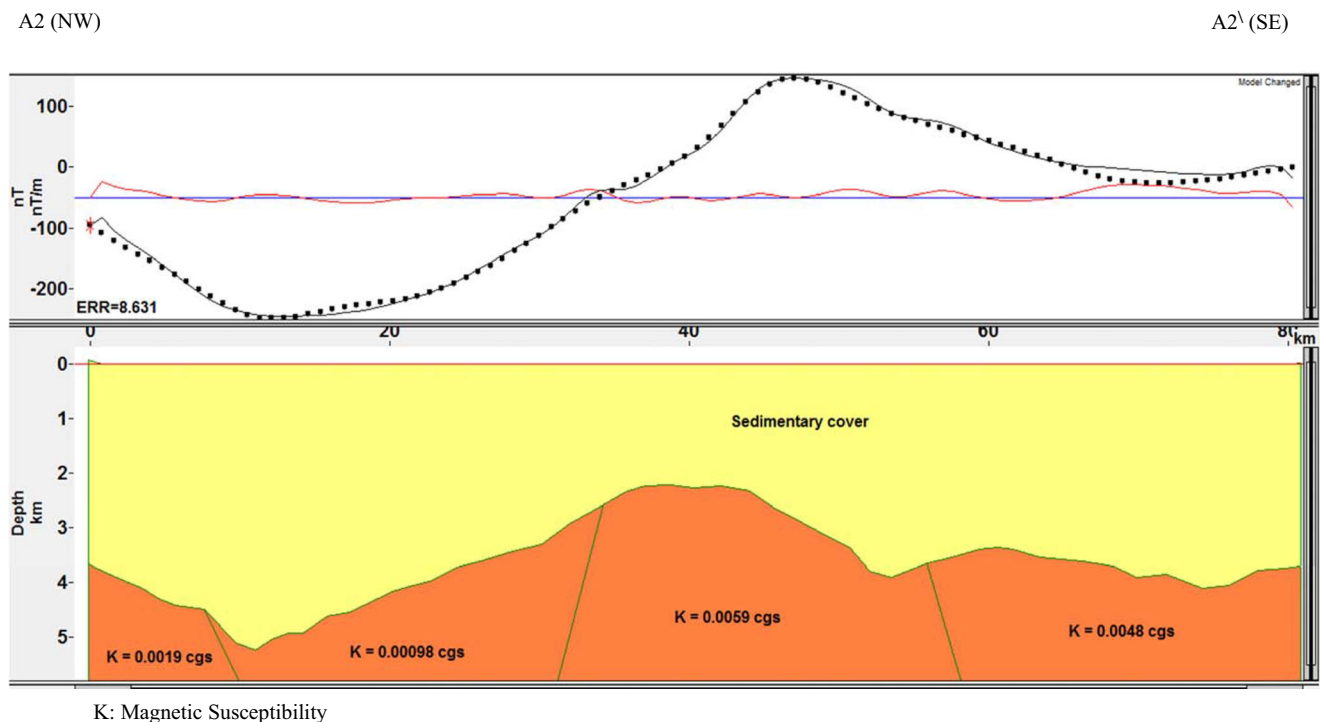

K: Magnetic Susceptibility

Fig. 15 2.5D model of the second profile A2-A2$^\backslash$

component calculated from the power spectrum is about 4730 m, while the depth of residual component is about 1830 m; the depths of magnetic sources calculated by SPI range from 1857 to 4000 m; in Euler deconvolution, the calculated depths range from 1000 to 5000 m. Finally, the forward modeling shows that the depth to the basement surface ranging from 1200 to 5080 m in the first model and 2210 to 5220 m in the second model. The depths calculated from the previous techniques are in a good agreement with the depth to the basement reached from boreholes (DIYUR-1 borehole, the basement was reached at 1625 m; and BAHARYIA-1 borehole, the basement depth was about 1842 m).

Compliance with ethical standards

References

Aboud E, Salem A, Mekkawi M (2011) Curie depth map for Sinai Peninsula, Egypt deduced from the analysis of magnetic data. Tectonophysics 506:46–54

Aero-Service (1984) Final operational report of airborne magnetic/radiation survey in the Eastern Desert, Egypt. For the Egyptian General Petroleum Corporation (EGPC) and the Egyptian Geological Survey and Mining Authority (EGSMA), Aero-Service Division, Houston, Texas, USA, Six Volumes

Al-Badani M.A, Al-Wathaf Y.M (2017) Using the aeromagnetic data for mapping the basement depth and contact locations, at southern part of Tihamah region, western Yemen. Egypt J Pet 27(4):485–495

Al-Garni MA (2010) Magnetic survey for delineating subsurface structures and estimating magnetic sources depth, Wadi Fatima, KSA. J King Saud Univ Sci 22:87–96

Beadnell HJL (1905) The topography and geology of the Fayum Province of Egypt. Survey Department of Egypt, Cairo 101

Conoco (1986) Geological map of Egypt, Scale (1:500,000), NH 35 SE-Bahariya sheet

Deng Y, Chen Y, Wang P, Essa KS, Xub T, Liang X, Badal J (2016) Magmatic underplating beneath the Emeishan large igneous province (South China) revealed by the COMGRA-ELIP experiment. Tectonophysics 672–673:16–23

El Sirafie A.M (1986) Application of aeromagnetic, aeroradiometric and gravimetric survey data in the interpretation of the geology of Cairo-Baharyia area, North Western Desert, Egypt. Ph.D. thesis, Ain Shams University 154p

Elkhodary ST, Youssef MAS (2013) Integrated potential field study on the subsurface structural characterization of the area North Bahariya Oasis, Western Desert, Egypt. Arab J Geosci 6:3185–3200

Eppelbaum LV (2015) Quantitative interpretation of magnetic anomalies from bodies approximated by thick bed models in complex environments. Environ Earth Sci 74(7):5971–5988

Essa KS, Elhussein M (2016) A new approach for the interpretation of magnetic data by a 2-D dipping dike. J Appl Geophys 136:431–443

Fairhead J.D, Williams S.E, Flanagan G (2004) Testing magnetic local wavenumber depth estimation methods using a complex 3D test model. 74th Annual International Meeting, SEG Expand Abstr. 742e745

Gabtni H, Hajjia O, Jalloulibc C (2016) Integrated application of gravity and seismic methods for determining the dip angle of a fault plane: case of Mahjouba fault (Central Tunisian Atlas Province, North Africa). J Afr Earth Sci 119:160–170

Kusky TM, Hassaan MM, Gabr S (2011) Structural and tectonic evolution of El-Faiyum Depression, North Western Desert, Egypt based on analysis of Landsat ETM+, and SRTM data. J Earth Sci 22(1): 75–100

Li X (2008) Magnetic reduction-to-the-pole at low latitudes: observations and considerations. Lead Edge 27(8). https://doi.org/10.1190/1.2967550

MacLeod IN, Jones K, Dai TF (1993) 3-D analytic signal in the interpretation of total magnetic field Data at low magnetic latitudes. Explor Geophys 24(3–4):679–687

Maineult A (2016) Estimation of the electrical potential distribution along metallic casing from surface self-potential profile. J Appl Geophys 129:66–78

Mehanee S (2014) Accurate and efficient regularized inversion approach for the interpretation of isolated gravity anomalies. Pure Appl Geophys 171(8):1897–1937

Mehanee S, Zhdanov M (2002) Two-dimensional magnetotelluric inversion of blocky geoelectrical structures. J Geophys Res Solid Earth 107(B4):EPM 2–1–EPM: 2–11

Miller HG, Singh V (1994) Potential field tilt—a new concept for location of potential field sources. J Appl Geophys 32:213–217

Oasis Montaj Program v7.1. (2009) Geosoft mapping and processing system, version 7.1

Ogunmola JK, Ayolabi EA, Olobaniyi SB (2016) Structural-depth analysis of the Yola Arm of the Upper Benue Trough of Nigeria using high resolution aeromagnetic data. J Afr Earth Sci 124:32–43

Oruç B, Selim HH (2011) Interpretation of magnetic data in the Sinop area of Mid Black Sea, Turkey, using tilt derivative, Euler deconvolution, and discrete wavelet transform. J Appl Geophys 74(4):194–204

Paoletti V, Ialongo S, Florio G, Fedi M, Cella F (2013) Self-constrained inversion of potential fields. Geophys J Int 195:854–869

Pei J, Li H, Wang H, Si J, Sun Z, Zhou Z (2014) Magnetic properties of the Wenchuan earthquake fault scientific drilling project Hole-1 (WFSD-1), Sichuan Province, China. Earth Planet. Space 66(23): 1–12

Rama Rao C, Kishore RK, Pradeep Kumar V, Butchi Babu B (2011) Delineation of intra crustal horizon in Eastern Dharwar Craton – an aeromagnetic evidence. J Asian Earth Sci 40(2):534–541

Reddi AGB, Mathew MP, Baldau S, Naidu PS (1988) Aeromagnetic evidence of crustal structure in the granulite terrane of Tamil Nadu–Kerala. J Geol Soc India 32:368–381

Reford MS, Sumner JS (1964) Aeromagnetics. Geophysics 29(4):482–516

Reid AB, Alsop JM, Grander H, Millet AJ, Somerton IW (1990) Magnetic interpretation in three dimensions using Euler deconvolution. Geophysics 55(1):80–91

Roest WR, Pilkington M (1993) Identifying remanent magnetization effects in magnetic data. Geophysics 58:653–659

Roset WR, Verhoef J, Pilkington M (1992) Magnetic interpretation using 3-D analytic signal. Geophysics 57:116–125

Saad MH, El-Khadragy AA, Shabaan MM, Azab A (2010) An integrated study of gravity and magnetic data on South Sitra area, Western Desert, Egypt. J Appl Sci Res 6(6):616–636

Said R (1962) The geology of Egypt. Elsevier, Amsterdam, p 377

Salawu N.B, Olatunji S, Orosun M.M, Abdulraheem T.Y (2019a) Geophysical inversion of geologic structures of Oyo Metropolis, Southwestern Nigeria from airborne magnetic data Geomechanics and Geophysics for Geo-Energy and Geo-Resources, https://doi.org/10.1007/s40948-019-00110-7

Salawu NB, Olatunji S, Adebiyi LS, Olasunkanmi NK, Dada SS (2019b) Edge detection and magnetic basement depth of Danko area, northwestern Nigeria, from low-latitude aeromagnetic anomaly data. SN Appl Sci 1:1056. https://doi.org/10.1007/s42452-019-1090-3

Salem A, Williams S, Fairhead JD, Ravat D, Smith R (2007) Tilt depth method, a simple depth estimation method using first-order magnetic derivatives. Lead Edge 26(12):1502–1505

Selim EI (2016) The integration of gravity, magnetic and seismic data in delineating the sedimentary basins of northern Sinai and deducing their structural controls. J Asian Earth Sci 115:345–367

Selim E, Aboud E (2012) Determination of sedimentary cover and structural trends in the Central Sinai area using gravity and magnetic data analysis. J Asian Earth Sci 43:193–206

Sheriff SD (2010) Matched filter separation of magnetic anomalies caused by scattered surface debris at archaeological sites. Near Surface Geophysics 8:145–150

Spector A, Grant FS (1970) Statistical models for interpreting aeromagnetic data. Geophysics 35(2):293–302

Talwani M, Heirtzler J.R (1964) Computation of magnetic anomalies caused by two-dimensional bodies of two-arbitrary shape. In: Parks, G.A. (Ed.), Computers in the mineral industries, part 1. In: Stanford University publications, geological sciences 9: 464–480

Thompson DT (1982) EULDPH—a technique for making computer-assisted depth estimates from magnetic data. Geophysics 47:31–37

Thurston JB, Smith RS (1997) Automatic conversion of magnetic data to depth, dip, and susceptibility contrast using the SPI (TM) method. Geophysics 62(3):807–813

Verduzco B, Fairhead JD, Green CM, Mackenzie C (2004) New insights into magnetic derivatives for structural mapping. Lead Edge 23(2): 116–119

Vondra CF (1974) Upper Eocene transitional and near-shore marine Qasr El Sagha Formation, Fayum Depression, Egypt. Ann Geol Surv Egypt 4:74–94

Zhdanov MS, Ellis R, Mukherjee S (2004) Three-dimensional regularized focusing inversion of gravity gradient tensor component data. Geophysics 69(4):925–937